# Model Analysis and Sliding Mode Current Controller for Multilevel Railway Power Conditioner Under the V/v Traction System

Fujun Ma, *Member, IEEE*, Zhen Zhu, Jun Min, *Student Member, IEEE*, Yufei Yue, and Xianxian He

***Abstract*—To manage the power quality of a high-speed V/v traction system, a multilevel railway power conditioner (MRPC) is researched. According to the structure and equivalent models of the MRPC, basically the MRPC is a symmetrical system, and its four clusters can be divided into two cluster groups. According to the ac equivalent mathematical models of cluster groups, it can be considered as the relationships in the $\alpha\beta$ frame, but not completely symmetrical, so the positive- and negative-sequence *dq* models for cluster groups can be derived. As the fluctuation and randomness of the locomotive loads, a sliding mode control system based on the exponential reaching law in the *dq* frame is explored to control the cluster ac currents, which can improve the dynamic performance and keep a good tolerance against parameter mismatches. Finally, an experimental prototype is developed, and the results show the feasibility and the robustness of the system.**

***Index Terms*—Circuiting current, modular multilevel converter (MMC), power quality, railway power conditioner, sliding mode control (SMC).**

## I. Introduction

OVER THE years, the electrified railway, especially the high-speed railway, has made a rapid development. The traction features of the electrified railway cause some serious power quality problems such as negative sequence currents (NSCs), and harmonics and voltage fluctuations of the traction system, so it is significant to govern the power quality of the railway traction system. Currently, to manage power quality problems, different methods have been studied according to the features of the traction system. Some balance transformers and power electronic transformers are used to achieve the balance of active power and reduce NSCs [1]–[4]. Meanwhile, in the governance of reactive power and harmonics, passive filter, static var compensator (SVC), static synchronous compensator, and hybrid active power filters are commonly used [5]–[8]. Then, in 1993, the concept of a railway power regulator (RPC) was proposed by scholars [9], which consists of two back-to-back

Manuscript received November 29, 2017; revised February 12, 2018 and April 2, 2018; accepted May 4, 2018. Date of publication May 10, 2018; date of current version December 7, 2018. This work was supported by the National Natural Science Foundation of China under Grant 51607062. Recommended for publication by Associate Editor Z. Li. *(Corresponding author: Fujun Ma.)*

The authors are with the College of Electrical and Information Engineering, Hunan University, Changsha 410082, China (e-mail:

of operating conditions. Kaleybar *et al*. [24] proposed a new extraction method to keep a fast dynamic and high accuracy response, which is based on modified instantaneous reactive power theory. In [25], a recessive self-tuning PI controller in the current control system was proposed to keep the dynamic performance. In [26] and [27], a model predictive control method and a passivity-based control method were proposed, respectively, for a fast dynamic response of power compensation. From the descriptions of the aforementioned, some advanced control techniques have already successfully applied to the compensation and control of a high-speed railway system. However, sliding mode control (SMC) could also be proved to be an effective method because of its robustness, stability, and good dynamic response with the inherent switching nature [28]–[31], and it is rarely applied and mentioned in the high-speed railway system, where the operation conditions are frequently varied. In [32], Gao and Hung focused on the reaching condition, and first proposed the concept of the reaching law, which increased the robustness and the stability of the system. In [33], Yong *et al*. proposed that an SM controller has a chattering problem and high switching frequency, and to suppress the chattering, seven solutions were proposed, which can provide guidance for the engineering. In [34]–[36], the SM controller was successfully adopted in electric drives systems for direct torque control. And in [30] and [37], the SM controller was also prosperously applied to pulsewidth modulation (PWM) inverters in the renewable energy sources. All the SMC techniques have developed rapidly and applied to many nonlinear systems successfully. Therefore, to improve the robustness and dynamic performance of the system, an SMC system in the *dq* frame is explored for the MRPC here. In the design of the SM controller, taking the uncertainty of the system into account, the closed-loop control system should still maintain the stability and ensure the appropriate dynamic performance when a certain range of uncertain parameters and a certain limitation of load dynamics exist.

The structure of this paper is as follows. In Section II, the working principle and mathematical models of the MRPC are derived. In Section III, according to the model of the V/v traction system, the control system is divided into two parts, one is the cluster-group SM current control in positive- and negative-sequence *dq* frames, which is derived to achieve active power transferring and NSC compensation; the other is the cluster-group circuiting-current control to achieve the power rebalance among the clusters and suppress the voltage divergence. The experimental sections and conclusions are presented in Section IV and V, respectively.

## II. Model and Working Principle of the MRPC

The main circuit topology of the MRPC is shown in Fig. 1. The MRPC is composed of four clusters; each H-bridge cluster is formed by the cascaded H-bridge cells. According to the symmetrical feature, the four clusters can be divided into two groups. Cluster 1 (C1) and cluster 4 (C4) can be classified as group 1, while cluster 2 (C2) and cluster 3 (C3) can be classified as group 2. The MRPC can be connected to the *a*/*b* phase

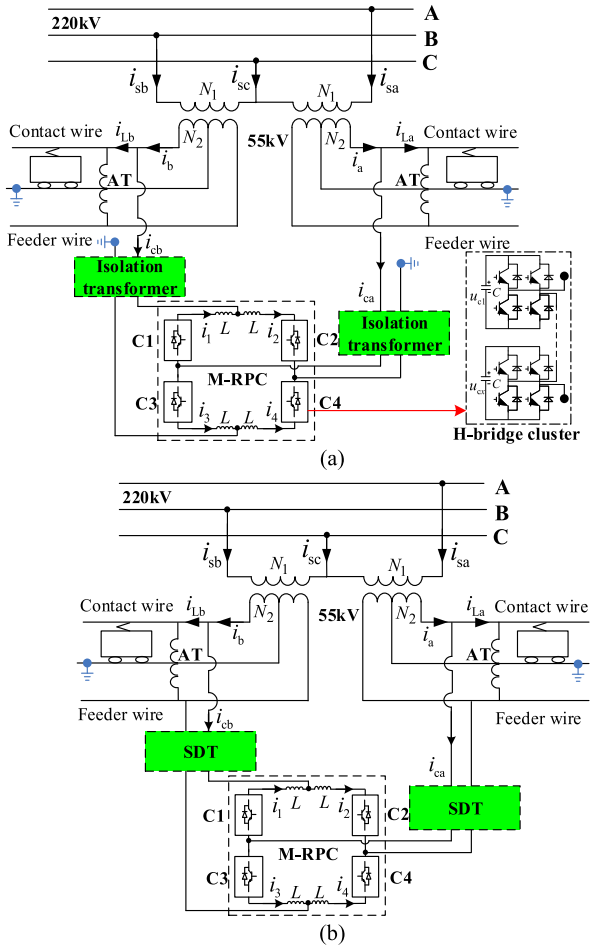


Fig. 1. Schematic of AT-mode-based traction systems. (a) A mode. (b) B mode.

contact wires and ground, and the isolation transformers (ITs) are needed to prevent the short-circuiting of some clusters in the MRPC, as shown in Fig. 1(a). Ideally, the ATs will not affect the compensation of the MRPC. If it is applied in the cophase traction power system, the MRPC can be directly connected with the traction power feeders without ITs. There is another kind of auto-transformer (AT)-mode based traction systems in Fig. 1(b), and the MRPC can be directly connected to the 55 kV bus without the IT. However, considering the series module number and system reliability, it is suggested to be installed with a proper SDT, which can make the operation of the MRPC more safe and reliable. So, the MMC technology is adopted to achieve high-power compensation, which can improve the operation performance of the compensator.

From Fig. 1(a), the ac and dc equivalent circuits of the MRPC can be obtained [16] and shown in Fig. 2, where $u_a$ and $u_b$ are the secondary voltage of the V/v transformer, $i_{\rm ca}$ and $i_{\rm cb}$ are the two-phase output currents of the MRPC, $u_{\rm x}$ $(x = 1, 2, 3, 4)$ is the output voltage of cluster $x$, $i_{\rm x}$ is the current of cluster $x$, $L$ is the filter inductance, and $R$ is the resistance of the cluster.

According to Kirchhoff voltage and current laws and taking the equivalent circuits of the MRPC into account, the mathe-

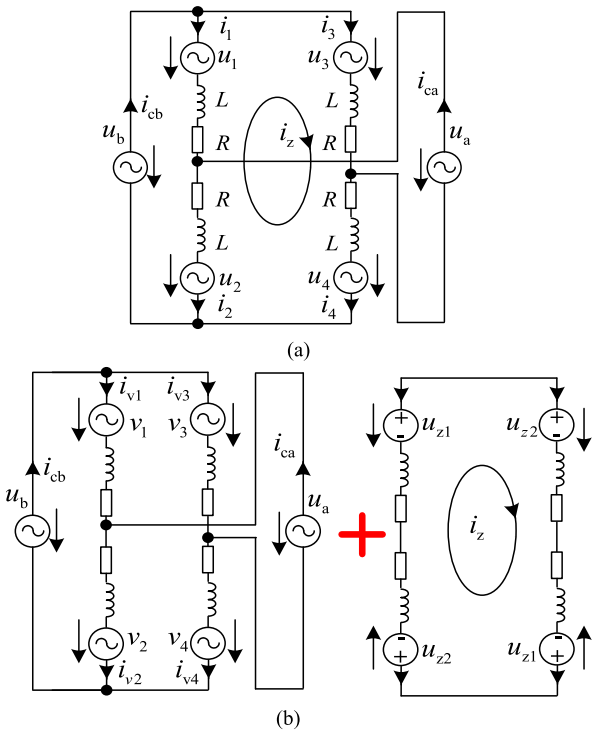


Fig. 2. Equivalent circuit of the MRPC. (a) Overall equivalent circuit. (b) AC + DC equivalent circuit.

matical models of two cluster groups can be obtained

$$\begin{cases} u_b - u_a = u_1 + u_4 + L\frac{d(i_1+i_4)}{dt} + R(i_1+i_4) \\ u_b + u_a = u_2 + u_3 + L\frac{d(i_2+i_3)}{dt} + R(i_2+i_3) \end{cases} \tag{1}$$

$$\begin{cases} i_1 = i_{v1} - i_z, i_4 = i_{v4} + i_z \\ i_2 = i_{v2} - i_z, i_3 = i_{v3} + i_z \end{cases} ; \begin{cases} i_{v1} = i_{v4} = (i_{cb} - i_{ca})/2 \\ i_{v2} = i_{v3} = (i_{cb} + i_{ca})/2 \\ i_z = (i_3 + i_4 - i_1 - i_2)/4 \end{cases} \tag{2}$$

$$\begin{cases} u_1 = v_1 + u_{z1}, u_4 = v_4 - u_{z1} \\ u_2 = v_2 - u_{z2}, u_3 = v_3 + u_{z2} \end{cases} \tag{3}$$

where $i_{v1}, i_{v2}, i_{v3}, i_{v4}$ are the ac component of $i_1, i_2, i_3, i_4$; $i_z$ is the dc component; $v_1, v_2, v_3, v_4$ are the ac component of $u_1, u_2, u_3, u_4$; $u_{z1}, u_{z2}$ are the dc component, and in the steady state, $u_{z1} \approx u_{z2}$. According to the mathematical model, it can be seen that the MRPC basically is a symmetrical system, and the ac components of clusters 1 and 2 are equal to the ones of clusters 4 and 3, respectively. So here, clusters 1 and 4 are classified as group 1 and clusters 3 and 2 are classified as group 2. According to (1) and (2)

$$\begin{cases} v_{1,4} = e_a - Ldi_{v1,4}/dt - Ri_{v1,4} \\ v_{2,3} = e_b - Ldi_{v2,3}/dt - Ri_{v2,3} \end{cases} \tag{4}$$

where $e_a = [(u_b - u_a)/2]$ is the differential-mode voltage, and $e_b = [(u_b + u_a)/2]$ is the common-mode voltage. According to the dc equivalent model, the circulating voltages $u_{z1}, u_{z2}$ will meet

$$u_{z1} - u_{z2} = 2L * di_z/dt + 2i_z R. \tag{5}$$

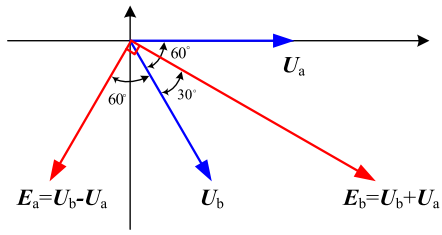


Fig. 3. Voltage vector diagram.

According to [16], a dc circulating current is adopted for the MRPC and injected into the two cluster groups, and it can achieve the rebalance of active power of two cluster groups and maintain the cluster-group voltage stable and balanced.

From (1) to (5), it can be seen that by controlling the output voltages of the four clusters, the current $i_x$ of each cluster can be controlled, which can not only achieve the indirect control of output currents $i_{ca}, i_{cb}$, but also control the internal circulating current of the MRPC independently, because the ac and dc components are decoupling.

## III. Control Strategy

The number of locomotives on the traction feeder is varied, and load power of locomotives is fluctuating. To improve the dynamic performance and the robustness against the change in parameter, an SMC in the *dq* frame is discussed to achieve a rapid tracking control of the current reference signals. According to the model of the V/v traction system, the control system is divided into two parts, one is the cluster-group ac control to achieve active power transfer and negative-sequence compensation; the other is the cluster-group dc current control to achieve the power rebalance within the groups and suppress the voltage divergence, which can maintain the voltage balance of clusters. The control method of the system is as follows.

### A. AC Current Control in the Cluster Groups

*1) DQ Model of the MRPC and Structure Design of SMC:* Aiming at the fluctuation and randomness of the high-speed railway system, an SMC system under the *dq* frame is explored to improve the dynamic tracking performance and the robustness of the system. The SMC is aimed at the output currents of the MRPC, which can make the MRPC accurately compensate the negative-sequence currents of the railway system.

According to the feature of the V/v traction system, the amplitude of $u_b$ and $u_a$ is equal and the phase difference is 60°. As shown in the vector diagram, $e_a$ and $e_b$ can be obtained. They are perpendicular to each other, but their amplitudes are different. Therefore, (4) can be considered as the relationships in the $\alpha\beta$ frame, but the ac components are not completely symmetrical, so they can be decomposed into positive-sequence and negative-sequence components, as shown in Fig. 3.

By detecting the synchronous signals $e_a$ and $e_b$ and normalizing them, $-\cos\theta$ and $\sin\theta$ can be obtained and form the $\alpha\beta/dq$ matrix **Park2** as follows:

$$\mathbf{Park2}(\theta) = \begin{bmatrix} \cos\theta & \sin\theta \\ -\sin\theta & \cos\theta \end{bmatrix}. \tag{6}$$

Using the $\alpha\beta/dq$ matrixes $\mathbf{Park2}(\theta)$ and $\mathbf{Park2}(-\theta)$, according to (4), the mathematical models of the MRPC in the *dq* synchronous frame can be deduced

$$\begin{cases} L\frac{di_{1\mathrm{d}}}{dt} = e_{1\mathrm{d}} + \omega L i_{1\mathrm{q}} - R i_{1\mathrm{d}} - v_{1\mathrm{d}} \\ L\frac{di_{1\mathrm{q}}}{dt} = e_{1\mathrm{q}} - \omega L i_{1\mathrm{d}} - R i_{1\mathrm{q}} - v_{1\mathrm{q}} \end{cases} \tag{7}$$

$$\begin{cases} L\frac{di_{2\mathrm{d}}}{dt} = e_{2\mathrm{d}} - \omega L i_{2\mathrm{q}} - R i_{2\mathrm{d}} - v_{2\mathrm{d}} \\ L\frac{di_{2\mathrm{q}}}{dt} = e_{2\mathrm{q}} + \omega L i_{2\mathrm{d}} - R i_{2\mathrm{q}} - v_{2\mathrm{q}} \end{cases} \tag{8}$$

where $e_{1\mathrm{d}}, e_{1\mathrm{q}}, e_{2\mathrm{d}}, e_{2\mathrm{q}}$ represent the positive-and negative-sequence components of $e_a$ and $e_b$, respectively; $v_{1\mathrm{d}}, v_{1\mathrm{q}}, v_{2\mathrm{d}}, v_{2\mathrm{q}}$ denote the positive-and negative-sequence components of $v_{1,4}$ and $v_{2,3}$, respectively; $i_{1\mathrm{d}}, i_{1\mathrm{q}}, i_{2\mathrm{d}}, i_{2\mathrm{q}}$ represent the positive- and negative-sequence components of $i_{v1,4}$ and $i_{v2,3}$, respectively; and $\omega$ is the fundamental frequency of the system.

As the complexity of the high-speed railway system is increasing, and its operating environment varies from time to time, so it is unrealistic and even impossible to design the control system with precise mathematical models. To enhance the robustness of the system, an SMC with the exponential reaching law in the *dq* frame is studied. According to the SMC, the four sliding surfaces can be designed to achieve the tracking control of the cluster currents in the *dq* synchronous frame as follows:

$$\begin{cases} S_{1\mathrm{d}} = i_{1\mathrm{d}} - i_{1\mathrm{dref}} \\ S_{1\mathrm{q}} = i_{1\mathrm{q}} - i_{1\mathrm{qref}} \\ S_{2\mathrm{d}} = i_{2\mathrm{d}} - i_{2\mathrm{dref}} \\ S_{2\mathrm{q}} = i_{2\mathrm{q}} - i_{2\mathrm{qref}} \end{cases} \tag{9}$$

where $i_{1\mathrm{dref}}, i_{1\mathrm{qref}}, i_{2\mathrm{dref}}$, and $i_{2\mathrm{qref}}$ are the references of $i_{1\mathrm{d}}$, $i_{1\mathrm{q}}$, $i_{2\mathrm{d}}$, and $i_{2\mathrm{q}}$, respectively. Generally, the tracking performance is adopted to measure the effect of SMC, especially in the case of external interference. To allow the controlled variable to slide on the sliding surface, define the following sliding vector $\sigma$:

$$\sigma = \begin{bmatrix} S_{1\mathrm{d}} \\ S_{1\mathrm{q}} \\ S_{2\mathrm{d}} \\ S_{2\mathrm{q}} \end{bmatrix} = 0. \tag{10}$$

The equivalent control law should meet $\dot{\sigma} = 0$, namely

$$\dot{\sigma} = \begin{bmatrix} \dot{S}_{1\mathrm{d}} = \dot{i}_{1\mathrm{d}} - \dot{i}_{1\mathrm{dref}} \\ \dot{S}_{1\mathrm{q}} = \dot{i}_{1\mathrm{q}} - \dot{i}_{1\mathrm{qref}} \\ \dot{S}_{2\mathrm{d}} = \dot{i}_{2\mathrm{d}} - \dot{i}_{2\mathrm{dref}} \\ \dot{S}_{2\mathrm{q}} = \dot{i}_{2\mathrm{q}} - \dot{i}_{2\mathrm{qref}} \end{bmatrix} = 0. \tag{11}$$

The main drawback of SMC is the chattering problem caused by the discontinuous control. Some kinds of reaching laws proposed by Gao and Hung can weaken the chattering [32]. Here, the exponential reaching law is studied, and it can be developed in the matrix form as

$$\dot{\sigma} = -\begin{bmatrix} \varepsilon_{1\mathrm{d}} & \mathrm{sgn}(S_{1\mathrm{d}}) + k_{1\mathrm{d}} S_{1\mathrm{d}} \\ \varepsilon_{1\mathrm{q}} & \mathrm{sgn}(S_{1\mathrm{q}}) + k_{1\mathrm{q}} S_{1\mathrm{q}} \\ \varepsilon_{2\mathrm{d}} & \mathrm{sgn}(S_{2\mathrm{d}}) + k_{2\mathrm{d}} S_{2\mathrm{d}} \\ \varepsilon_{2\mathrm{q}} & \mathrm{sgn}(S_{2\mathrm{q}}) + k_{2\mathrm{q}} S_{2\mathrm{q}} \end{bmatrix} \tag{12}$$

where $\varepsilon_{xy}$ and $k_{xy}$ ($x = 1, 2$ and $y = d, q$) are the SMC parameters. According to the exponential reaching law under the *dq* mathematical model of the MRPC, the following equation can be considered for the SMC system:

$$\begin{cases} -\varepsilon_{1\mathrm{d}} \ \mathrm{sgn}(S_{1\mathrm{d}}) - k_{1\mathrm{d}} S_{1\mathrm{d}} = L * di_{1\mathrm{d}}/dt \\ -\varepsilon_{1\mathrm{q}} \ \mathrm{sgn}(S_{1\mathrm{q}}) - k_{1\mathrm{q}} S_{1\mathrm{q}} = L * di_{1\mathrm{q}}/dt \\ -\varepsilon_{2\mathrm{d}} \ \mathrm{sgn}(S_{2\mathrm{d}}) - k_{2\mathrm{d}} S_{2\mathrm{d}} = L * di_{2\mathrm{d}}/dt \\ -\varepsilon_{2\mathrm{q}} \ \mathrm{sgn}(S_{2\mathrm{q}}) - k_{2\mathrm{q}} S_{2\mathrm{q}} = L * di_{2\mathrm{q}}/dt. \end{cases} \tag{13}$$

As the resistance $R$ of the H-bridge cluster is small, it can be ignored. There is

$$\begin{cases} -\varepsilon_{1\mathrm{d}} \ \mathrm{sgn}(S_{1\mathrm{d}}) - k_{1\mathrm{d}} S_{1\mathrm{d}} = e_{1\mathrm{d}} + \omega L i_{1\mathrm{q}} - v_{1\mathrm{d}} \\ -\varepsilon_{1\mathrm{q}} \ \mathrm{sgn}(S_{1\mathrm{q}}) - k_{1\mathrm{q}} S_{1\mathrm{q}} = e_{1\mathrm{q}} - \omega L i_{1\mathrm{d}} - v_{1\mathrm{q}} \\ -\varepsilon_{2\mathrm{d}} \ \mathrm{sgn}(S_{2\mathrm{d}}) - k_{2\mathrm{d}} S_{2\mathrm{d}} = e_{2\mathrm{d}} - \omega L i_{2\mathrm{q}} - v_{2\mathrm{d}} \\ -\varepsilon_{2\mathrm{q}} \ \mathrm{sgn}(S_{2\mathrm{q}}) - k_{2\mathrm{q}} S_{2\mathrm{q}} = e_{2\mathrm{q}} + \omega L i_{2\mathrm{d}} - v_{2\mathrm{q}}. \end{cases} \tag{14}$$

The equivalent control law can be derived from (14), and there is

$$\begin{cases} v_{1\mathrm{d}} = e_{1\mathrm{d}} + \omega L i_{1\mathrm{q}} + \varepsilon_{1\mathrm{d}} \ \mathrm{sgn}(S_{1\mathrm{d}}) + k_{1\mathrm{d}} S_{1\mathrm{d}} \\ v_{1\mathrm{q}} = e_{1\mathrm{q}} - \omega L i_{1\mathrm{d}} + \varepsilon_{1\mathrm{q}} \ \mathrm{sgn}(S_{1\mathrm{q}}) + k_{1\mathrm{q}} S_{1\mathrm{q}} \\ v_{2\mathrm{d}} = e_{2\mathrm{d}} - \omega L i_{2\mathrm{q}} + \varepsilon_{2\mathrm{d}} \ \mathrm{sgn}(S_{2\mathrm{d}}) + k_{2\mathrm{d}} S_{2\mathrm{d}} \\ v_{2\mathrm{q}} = e_{2\mathrm{q}} + \omega L i_{2\mathrm{d}} + \varepsilon_{2\mathrm{q}} \ \mathrm{sgn}(S_{2\mathrm{q}}) + k_{2\mathrm{q}} S_{2\mathrm{q}}. \end{cases} \tag{15}$$

Here, the operation of the SMC system is based on a fixed switching frequency, and the exponential reaching law is studied for the SMC system, which can improve the dynamic performance and weaken the system chattering. Once the SMC is designed, then the reaching law ensuring system stability should be analyzed and explained.

*2) Stability and Its Arrival Conditions of SMC:* Take a derivative with (9), there is

$$\begin{cases} \dot{S}_{1\mathrm{d}} = \dot{i}_{1\mathrm{d}} - \dot{i}_{1\mathrm{dref}} \\ \dot{S}_{1\mathrm{q}} = \dot{i}_{1\mathrm{q}} - \dot{i}_{1\mathrm{qref}} \\ \dot{S}_{2\mathrm{d}} = \dot{i}_{2\mathrm{d}} - \dot{i}_{2\mathrm{dref}} \\ \dot{S}_{2\mathrm{q}} = \dot{i}_{2\mathrm{q}} - \dot{i}_{2\mathrm{qref}}. \end{cases} \tag{16}$$

Combining (7) with (8) and (15), there is (17) shown at the bottom of next page.

The goal of the arrival condition is to ensure that, regardless of the initial position, the corresponding control output will make the trajectory of the system to approach and eventually reach the sliding surface. The sufficient and necessary conditions for the system to satisfy the arrival condition are that the equivalent

control law $v_{d,q}$ produces a state variable $\boldsymbol{x}$ and the control trajectory $S$ should satisfy the following inequality:

$$S\dot{S} < 0. \tag{18}$$

Bringing (16) and (17) into (18), there is (19) shown at the bottom of this page.

The constraint conditions of the SMC parameters can be derived from (19), and there is

$$\begin{cases} k_{\mathrm{xd}} > 0 \\ k_{\mathrm{xq}} > 0 \end{cases}, \begin{cases} \varepsilon_{\mathrm{xd}} > \left| Ri_{\mathrm{xdref}} + L\dot{i}_{\mathrm{xdref}} \right| \\ \varepsilon_{\mathrm{xq}} > \left| Ri_{\mathrm{xqref}} + L\dot{i}_{\mathrm{xqref}} \right| \end{cases} \tag{20}$$

where $x = 1, 2$. The big control parameters would enlarge the chattering problem, while small values would affect the dynamic converging response. So here, a tradeoff is considered for the design of control parameters. The matrix of modulation signals $[v_{1\mathrm{d}}, v_{1\mathrm{q}}, v_{2\mathrm{d}}, v_{2\mathrm{q}}]^T$, which is the SMC output in the *dq* frame system, can be transformed by matrix $\mathbf{T_{Park4}}^{-1}$, and the following equation can be obtained:

$$\left[v_{1,4}^{+}, v_{2,3}^{+}, v_{1,4}^{-}, v_{2,3}^{-}\right]^T = T_{\mathrm{Park4}}^{-1} * [v_{1\mathrm{d}}, v_{1\mathrm{q}}, v_{2\mathrm{d}}, v_{2\mathrm{q}}]^T \tag{21}$$

where

$$\mathbf{T_{Park4^{-1}}} = \begin{bmatrix} \mathbf{T_{Park2(\theta)^{-1}}} & \begin{matrix} 0 & 0 \\ 0 & 0 \end{matrix} \\ \begin{matrix} 0 & 0 \\ 0 & 0 \end{matrix} & \mathbf{T_{Park2(-\theta)^{-1}}} \end{bmatrix}.$$

According to (15) and (21), the system-level SMC diagram can be obtained, as shown in Fig. 5. The SMC is developed to control the positive- and negative-sequence components in the *dq* frame, which can achieve a fast control of ac currents of two cluster groups to compensate negative-sequence currents.

*3) Equilibrium Point Acquisition in the DQ Frame:* According to the compensation principle of negative -sequence currents in the V/v traction system [38], the expected output currents of the MRPC can be obtained as follows:

$$\begin{cases} {i_{\mathrm{ca}}}^r = i_{La} - \left[ I_{\mathrm{m}} * \sin\left(\omega t - \frac{\pi}{6}\right) + \frac{\sqrt{3}}{3} I_{\mathrm{m}} * \sin\left(\omega t + \frac{\pi}{3}\right) \right] \\ {i_{\mathrm{cb}}}^r = i_{Lb} - \left[ I_{\mathrm{m}} * \sin\left(\omega t - \frac{\pi}{2}\right) + \frac{\sqrt{3}}{3} I_{\mathrm{m}} * \sin(\omega t - \pi) \right] \end{cases} \tag{22}$$

where $I_{\mathrm{m}} = (I_{ap} + I_{bp})/2$ is half of the sum of two active current amplitudes. According to the feature of the MRPC, the current reference of each cluster can be obtained as

$$\begin{cases} {i_{1,4}}^r = ({i_{\mathrm{cb}}}^r - {i_{\mathrm{ca}}}^r)/2 \\ {i_{2,3}}^r = ({i_{\mathrm{cb}}}^r + {i_{\mathrm{ca}}}^r)/2. \end{cases} \tag{23}$$

According to the analysis of the MRPC, the overall energy of the compensator is naturally balanced when ignoring its own loss. Due to the existence of switching losses and power loss of a resistor, the capacitor voltage of the cascaded cells will be reduced. Therefore, in the steady state, the MRPC has to absorb some active current from the traction feeders to maintain the submodule capacitor voltage balanced, which can be achieved by controlling the active current of each cluster.

The sum of the capacitor voltages $u_{c1}^{\Sigma}, u_{c2}^{\Sigma}, u_{c3}^{\Sigma}, u_{c4}^{\Sigma}$ of the cascaded cells corresponding to each cluster can be obtained by the detection link, and then the average value can be obtained as follows:

$$u_{\mathrm{dcave}} = \left(u_{c1}^{\Sigma} + u_{c2}^{\Sigma} + u_{c3}^{\Sigma} + u_{c4}^{\Sigma}\right)/4N \tag{24}$$

where $N$ is the number of H-bridge cells for each cluster. Then, the dc correction signal $\Delta I$ of the active current can be obtained by the PI controller using the voltage difference $(u_{d\mathrm{cave}} - \mathrm{u_{ref}})$, as shown in Fig. 4. The reference currents $i_{d1,4}^*$ and $i_{d2,3}^*$, which can keep the cluster voltage balanced, can be obtained separately by multiplying the dc signal with the synchronous signals $se_a$ and $se_b$, respectively. Therefore, the total ac reference signal for each cluster can be obtained as follows:

$$\begin{cases} {i_{1,4}}^* = i_{d1,4}^* + i_{1,4}^r = \Delta I * se_{\mathrm{a}} + ({i_{\mathrm{cb}}}^r - {i_{\mathrm{ca}}}^r)/2 \\ {i_{2,3}}^* = i_{d2,3}^* + i_{2,3}^r = \Delta I * se_b + ({i_{\mathrm{cb}}}^r + {i_{\mathrm{ca}}}^r)/2. \end{cases} \tag{25}$$

Therefore, the reference signal in the *dq* frame can be obtained by using matrix $T_{\mathbf{Park4}}$ to transform the reference signal matrix $[i_{1,4}^*, i_{2,3}^*, i_{1,4}^*, i_{2,3}^*]^T$, and there is

$$[i_{1\mathrm{dref}}, i_{1\mathrm{qref}}, i_{2\mathrm{dref}}, i_{2\mathrm{qref}}]^T = T_{\mathrm{Park4}} * \left[i_{1,4}^*, i_{2,3}^*, i_{1,4}^*, i_{2,3}^*\right]^T \tag{26}$$

$$\begin{cases} \dot{S}_{1\mathrm{d}} = -\frac{1}{L}(RS_{1\mathrm{d}} + Ri_{1\mathrm{dref}} + L\dot{i}_{1\mathrm{dref}} + \varepsilon_{1\mathrm{d}} \ \ \mathrm{sgn}(S_{1\mathrm{d}}) + k_{1\mathrm{d}}S_{1\mathrm{d}}) \\ \dot{S}_{1\mathrm{q}} = -\frac{1}{L}(RS_{1\mathrm{q}} + Ri_{1\mathrm{qref}} + L\dot{i}_{1\mathrm{qref}} + \varepsilon_{1\mathrm{q}} \ \ \mathrm{sgn}(S_{1\mathrm{q}}) + k_{1\mathrm{q}}S_{1\mathrm{q}}) \\ \dot{S}_{2\mathrm{d}} = -\frac{1}{L}(RS_{2\mathrm{d}} + Ri_{2\mathrm{dref}} + L\dot{i}_{2\mathrm{dref}} + \varepsilon_{2\mathrm{d}} \ \ \mathrm{sgn}(S_{2\mathrm{d}}) + k_{2\mathrm{d}}S_{2\mathrm{d}}) \\ \dot{S}_{2\mathrm{q}} = -\frac{1}{L}(RS_{2\mathrm{q}} + Ri_{2\mathrm{qref}} + L\dot{i}_{2\mathrm{qref}} + \varepsilon_{2\mathrm{q}} \ \ \mathrm{sgn}(S_{2\mathrm{q}}) + k_{2\mathrm{q}}S_{2\mathrm{q}}). \end{cases} \tag{17}$$

$$\begin{cases} S_{1\mathrm{d}}\dot{S}_{1\mathrm{d}} = -\frac{1}{L}[(R + k_{1\mathrm{d}})S_{1\mathrm{d}}^2 + S_{1\mathrm{d}} * (\varepsilon_{1\mathrm{d}} \ \ \mathrm{sgn}(S_{1\mathrm{d}}) + Ri_{1\mathrm{dref}} + L\dot{i}_{1\mathrm{dref}})] < 0 \\ S_{1\mathrm{q}}\dot{S}_{1\mathrm{q}} = -\frac{1}{L}[(R + k_{1\mathrm{q}})S_{1\mathrm{q}}^2 + S_{1\mathrm{d}} * (\varepsilon_{1\mathrm{q}} \ \ \mathrm{sgn}(S_{1\mathrm{q}}) + Ri_{1\mathrm{qref}} + L\dot{i}_{1\mathrm{qref}})] < 0 \\ S_{2\mathrm{d}}\dot{S}_{2\mathrm{d}} = -\frac{1}{L}[(R + k_{2\mathrm{d}})S_{2\mathrm{d}}^2 + S_{2\mathrm{d}} * (\varepsilon_{2\mathrm{d}} \ \ \mathrm{sgn}(S_{2\mathrm{d}}) + Ri_{2\mathrm{dref}} + L\dot{i}_{2\mathrm{dref}})] < 0 \\ S_{2\mathrm{q}}\dot{S}_{2\mathrm{q}} = -\frac{1}{L}[(R + k_{2\mathrm{q}})S_{2\mathrm{q}}^2 + S_{2\mathrm{q}} * (\varepsilon_{2\mathrm{q}} \ \ \mathrm{sgn}(S_{2\mathrm{q}}) + Ri_{2\mathrm{qref}} + L\dot{i}_{2\mathrm{qref}})] < 0. \end{cases} \tag{19}$$

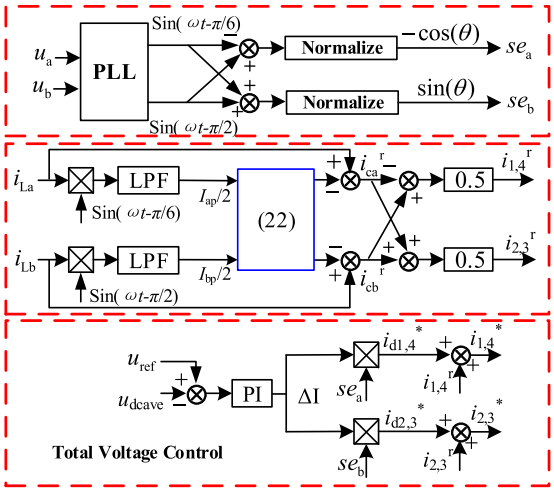


Fig. 4. Current reference acquisition of the MRPC.

where

$$\mathbf{T}_{\mathrm{Park4}} = \begin{bmatrix} \mathbf{T}_{\mathrm{Park2}}(\theta) & \begin{matrix} 0 & 0 \\ 0 & 0 \end{matrix} \\ \begin{matrix} 0 & 0 \\ 0 & 0 \end{matrix} & \mathbf{T}_{\mathrm{Park2}}(-\theta) \end{bmatrix}.$$

So, it can be obtained that the equilibrium points of the system in the *dq* frame are $[i_{1\mathrm{dref}}, i_{1\mathrm{qref}}, i_{2\mathrm{dref}}, i_{2\mathrm{qref}}]^T$.

### B. AC Current Control in the Cluster Groups

According to [16], when the MRPC is used to compensate reactive power of two traction arms, a positive dc active power $P_{\mathrm{d}}$ will be generated in clusters 1 and 4; meanwhile, a negative dc active power $-P_{\mathrm{d}}$ will be generated in clusters 2 and 3. There is

$$P_d = \sqrt{3}U * I_Q/8 \tag{27}$$

where $U$ is the voltage amplitude of the traction power arm, and $I_Q$ is the amplitude of the compensated reactive current. So, when the MRPC is used to compensate reactive currents in the V/v traction system, it is necessary to control the differences of active power of the clusters, which will bring on the divergence of the capacitor voltages between two cluster groups. Here, a dc circulating current injection method is adopted to achieve the active power rebalance and maintain the dc-link voltage stable, as shown in Fig. 5.

Here, $u_{\mathrm{cav}14}$ is defined as the average value of the capacitor voltages of group 1 composed of clusters 1 and 4, and $u_{\mathrm{cav}23}$ is defined as the average value of the capacitor voltages of group 2 composed of clusters 2 and 3. The following equation can be obtained:

$$\begin{cases} u_{\mathrm{cav}14} = (u_{c1}^{\Sigma} + u_{c4}^{\Sigma})/2N = (u_{\mathrm{cav}1} + u_{\mathrm{cav}4})/2 \\ u_{\mathrm{cav}23} = (u_{c2}^{\Sigma} + u_{c3}^{\Sigma})/2N = (u_{\mathrm{cav}2} + u_{\mathrm{cav}3})/2. \end{cases} \tag{28}$$

Assuming the circulating voltage reference is $u_{\mathrm{zref}}$, and then the feed-forward reference $i_{\mathrm{zref}}$ of dc circulating current can be calculated as $P_{\mathrm{d}}/u_{\mathrm{zref}}$. To eliminate the interference caused by the capacitor voltage deviation and the resistance $R$, the difference of the total capacitor voltages between groups 1 and 2 is fed into the PI controller, so a correction signal $\Delta i_{\mathrm{zref}}$ can be obtained. $\Delta i_{\mathrm{zref}}$ can be superimposed with $i_{\mathrm{zref}}$ to obtain the total reference signal $i_{\mathrm{zr}}$ of circulating current. As the circulating current $i_z$ is the direct current, PI can be used to achieve a rapid and accurate tracking of the reference, and then the correction signal $\Delta u_{\mathrm{z}}$ of the circulating voltage $u_{\mathrm{zref}}$ can be obtained. So, the circulating voltages $u_{\mathrm{z}1}$ and $u_{\mathrm{z}2}$ for groups 1 and 2 can be obtained

$$\begin{cases} u_{\mathrm{z}1} = (u_{\mathrm{zref}} + \Delta u_{\mathrm{z}}) \\ u_{\mathrm{z}2} = (u_{\mathrm{zref}} - \Delta u_{\mathrm{z}}). \end{cases} \tag{29}$$

Under the premise of voltage balance between two cluster groups, it is necessary to consider the voltage balance of H-bridge cells in each cluster. Here, the individual balance control is adopted for each cluster [26], [39], which can be achieved by carrier phase-shift modulation, as shown in Fig. 5. Summing up the output values of each layer of the controllers, the total modulation signal $m_{xy}$ for the *y*th H-bridge cell in the *x*th cluster can be obtained as follows:

$$\begin{cases} m_{1y} = (v_{1,4} + u_{\mathrm{z}1} + \Delta u_{1y})/u_{\mathrm{dcave}} \\ m_{2y} = (v_{2,3} - u_{\mathrm{z}2} + \Delta u_{2y})/u_{\mathrm{dcave}} \\ m_{3y} = (v_{2,3} + u_{\mathrm{z}2} + \Delta u_{3y})/u_{\mathrm{dcave}} \\ m_{4y} = (v_{1,4} - u_{\mathrm{z}1} + \Delta u_{4y})/u_{\mathrm{dcave}} \end{cases}, \begin{cases} v_{1,4} = {v_{1,4}}^{+} + {v_{1,4}}^{-} \\ v_{2,3} = {v_{2,3}}^{+} + {v_{2,3}}^{-} \end{cases}. \tag{30}$$

## IV. Verification

The experiments are carried out in this section to verify the effectiveness of the control methods and structures studied in this paper. A 380 V level prototype of the V/v traction system and the compensator is established in the laboratory. The physical structure of the device is given and described in Fig. 6. Two single-phase transformers are used as the V/v traction system, and the voltage of the traction power arm is 220 V. The pictures of the prototype system are shown in Fig. 7. Fig. 7(a) shows V/v traction power system and simulated loads, while Fig. 7(b) shows the prototype of RPC, DSP control board, and power module. Two single-phase isolated transformers are used for the MRPC, and two cascaded cells are adopted for each cluster. DSP2812 is used to sample signals and calculate the current control algorithm, and field programmable gate array is mainly used to output and drive PWM signals. The experimental parameters of the prototype are shown in Table I.

At first, the load is located at a phase-a traction power arm, and the MRPC is not enabled to output, so at this time there are a large amount of NSCs in the three-phase grid currents. And then the MRPC is enabled to transfer active power and compensate reactive power sequentially. The active power is transferred at 40 ms, and then the reactive power is compensated at 140 ms. The waveforms of three-phase grid currents and output currents of the MRPC are shown in Fig. 8(a). After compensation, the NSCs are significantly reduced and the three-phase grid currents are almost symmetrical. At this time, the unbalance level of three-

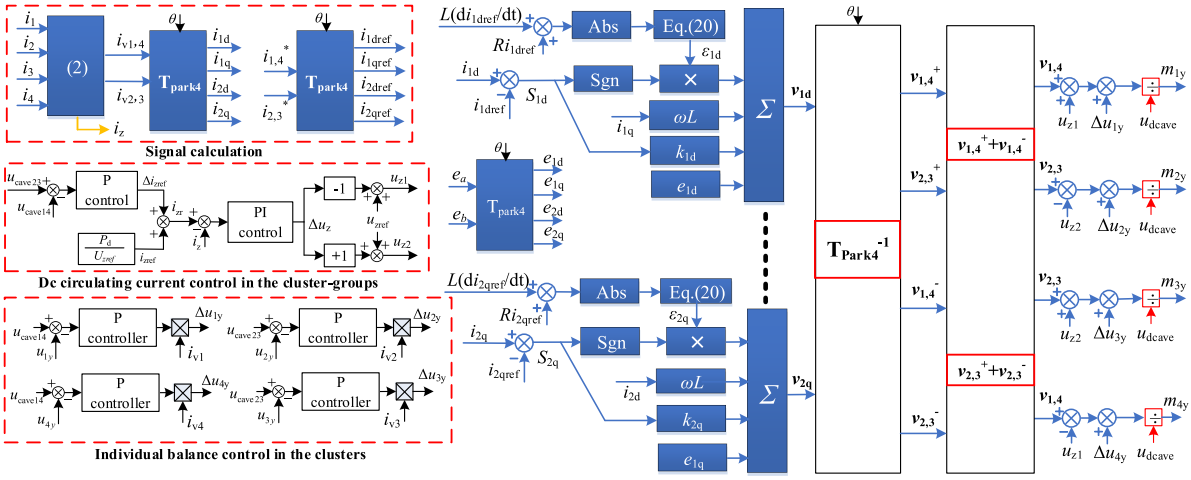


Fig. 5. System control diagram of the MRPC.

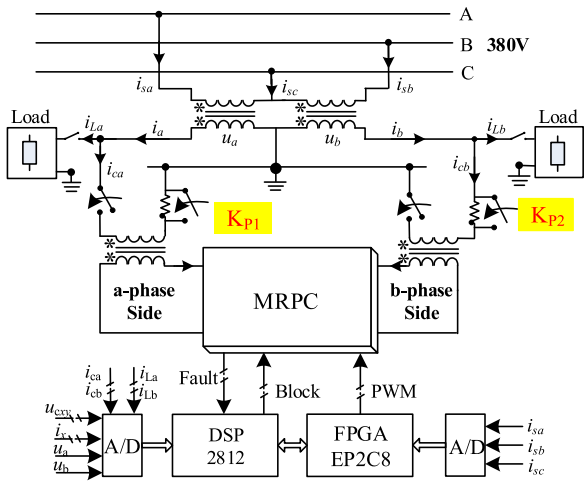


Fig. 6. Implementation diagram of the device.


(a)

(b)

Fig. 7. Picture of the prototype system. (a) V/v traction power system and simulated loads. (b) RPC's prototype, DSP control board, and power module.

TABLE I
EXPERIMENTAL PARAMETERS

| Symbol | PARAMETER | Value |
|---|---|---|
| $S$ | Locomotive capacity | 10/kW |
| $U_{rms}$ | Traction grid voltage | 220/V |
| $N$ | Number of modules per chain | 2 |
| $L$ | Link inductance | 2/mH |
| $C$ | Module capacitance value | 10/mF |
| $U_{dcref}$ | Capacitor voltage value | 200/V |
| $f_c$ | Carrier frequency | 2.5/kHz |

phase grid currents decreased from 100% to 3.66%. What is more, the grid voltage $u_{sa}$ and the grid currents $i_{sa}$ are shown in Fig. 8(b). It can be seen that the grid current is in the same phase with the grid voltage after compensation, which can justify the capability of the MRPC for reactive power compensation. The current waveforms for each cluster are shown in Fig. 8(c). When it is used for the transferring of active power, the cluster currents in each group are almost the same and the circuiting current is basically 0. Because of the reactive power compensation, a dc circuiting current is injected to achieve the rebalance of active power of each cluster, as shown in Fig. 8(d). The average capacitor voltages of each cluster are shown in Fig. 8(e), and the multilevel output voltage waveforms of each cluster are shown in Fig. 8(f). So, it can be seen that the capacitor voltages can be maintained stable during this period.

The results show that the MRPC can output the expected active and reactive currents to compensate the NSCs and improve the power quality of the railway traction system.

Due to the fluctuation of the railway loads, MRPC and its control system should be enhanced for the dynamic performance and the robustness. To verify the dynamic tracking effect of the SMC system, the locomotive load is simulated as sliding from phase-a power arm to phase-b power arm, and the experimental results are shown in Fig. 9. There is a neutral segment between two traction power arms. So, when the locomotive load enters this neutral segment, the load currents and grid currents will be 0, and the MRPC does not have to output. After 0.2 s, the locomotive load will enter the b-phase traction power arm, and

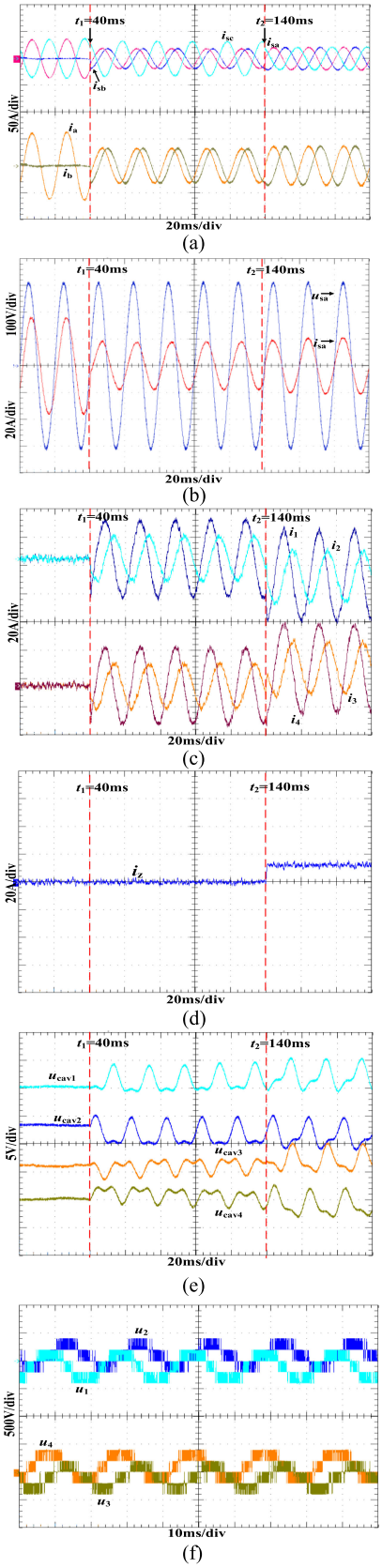


Fig. 8. Experimental waveforms before and after the compensation of the MPRC. (a) Three-phase grid currents and currents of two traction arms. (b) Grid voltage and current of phase a. (c) Currents of four clusters. (d) DC circuiting current. (e) Average capacitor voltages of each cluster. (f) Multilevel voltage waveforms of each cluster in the steady state.

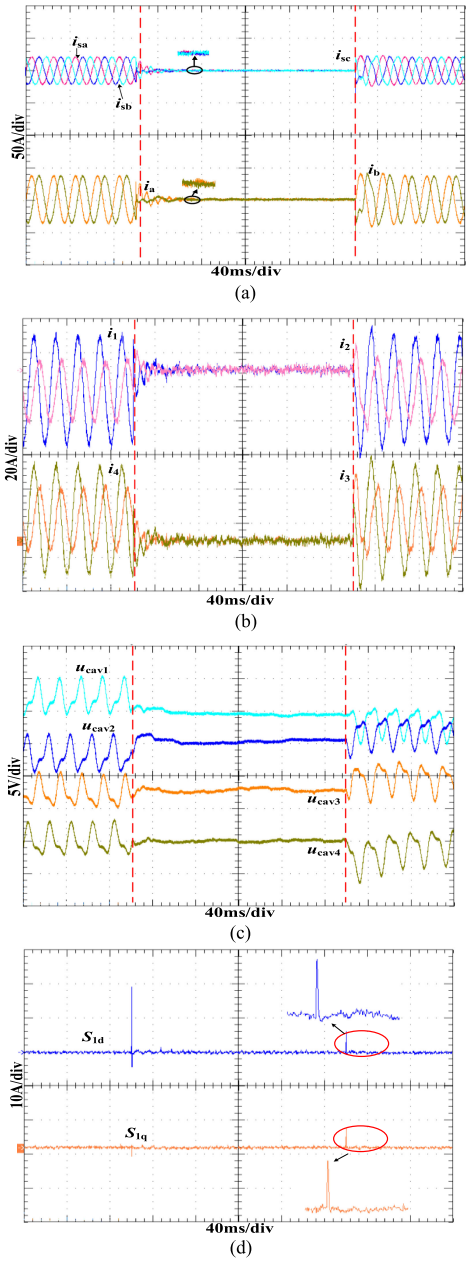


Fig. 9. Current tracking waveforms when the locomotive loads are fluctuated. (a) Three-phase grid currents and MRPC output currents. (b) Currents of four clusters. (c) Average capacitor voltages of each cluster. (d) Sliding surfaces $S_{1\mathrm{d}}$ and $S_{1\mathrm{q}}$.

then the MRPC will be put into compensation again, as shown in Fig. 9(a) and (b). The average capacitor voltages of each cluster are shown in Fig. 9(c), and they can be maintained stable during this period.

When the locomotive load departs from the a-phase traction power arm, the MRPC with the SMC can quickly reduce the output currents. Meanwhile, the locomotive load gets into the b-phase power arm, the MRPC is enabled to work and can rapidly increase the output currents, as shown in Fig. 9(b). Seen from Fig. 9(a) and (b), the system with SMC can almost recover to the steady state again within 30 ms. This response time includes the delay caused by sampling link and detection link of current

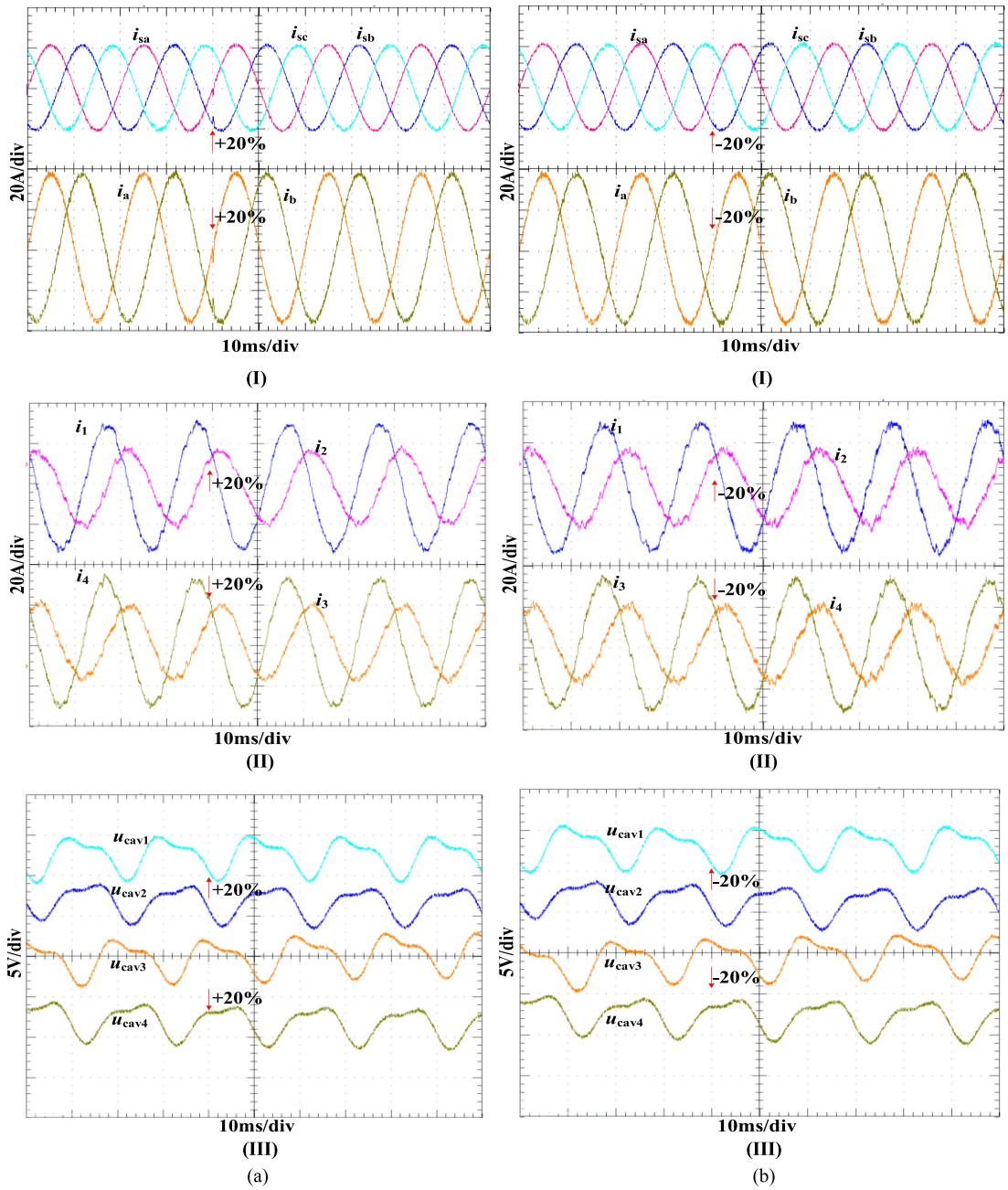


Fig. 10. Current tracking waveform of SMC under the parameter change condition. (a) When the error is +20%. (I) Three-phase grid currents and currents of two traction arms. (II) Four cluster currents. (III) Average capacitor voltages of each cluster. (b) When the error is –20%. (I) Three-phase grid currents and currents of two traction arms. (II) Four cluster currents. (III) Average capacitor voltages of each cluster.

references, and the low-pass filter of detection link is the main origin. It can be seen that the SMC with exponential reaching law can make the state variable rapidly return to the sliding surface when the error of state variable is far away from the sliding surface, as shown in Fig. 9(d). So, the SMC system can enhance the dynamic performance and guarantee a good control effect in the varied environment of traction loads.

To verify the robustness of the SMC system against the parameter change, a contrast experiment is carried out in the paper. The inductance $L$ in each link is changed and set to 20% and –20% of the nominal value, as shown in Fig. 10. It can be seen from Fig. 10(a-I) and (b-I) that when the filter inductance is changed suddenly, the MRPC with the SMC system can still track to the references rapidly and keep the waveforms of grid and traction currents well. The unbalance levels of grid currents are 3.54% and 3.76% when the parameter error of inductance is +20% and –20%, respectively.

In addition, the cluster currents and the cluster average capacitor voltages can be well controlled, as shown in Fig. 10(a-II), (a-III) and (b-II), (b-III). Therefore, SMC can enhance the robustness of the MRPC against the interference. When SMC is used, even if there are some mismatches in the system, the

MRPC can output reactive and active currents to compensate the NSCs normally, and it can maintain the stable operation of the system.

So, the MRPC with the SMC system can operate in the severe railway environment such as parameter mismatches and load fluctuations, to achieve the requirements of power quality compensation of the railway system.

## V. Conclusion

In this paper, first, the equivalent circuits of the MRPC under the V/v traction system are established and analyzed. According to the symmetrical feature of the MRPC, the mathematical models of two cluster groups can be considered as the relationships in an $\alpha\beta$ coordinate system, and then the positive- and negative-sequence *dq* models for two cluster groups can be derived. As the complexity of the high-speed railway system is increasing, and its operating environment varies from time to time, so it is unrealistic to design the control system with precise mathematical models. To enhance the robustness of the system, a SMC with the exponential reaching law in the *dq* frame is studied for the MRPC, which can achieve active power transferring and NSC compensation. In the presence of parameter uncertainties, the SMC system can keep stable and ensure the appropriate performance; meanwhile, it can alleviate the influence caused by the external disturbance.

## References


[1] A. A. Badin and I. Barbi, "Unity power factor isolated three-phase rectifier with split dc-bus based on the Scott transformer," *IEEE Trans. Power Electron.*, vol. 23, no. 3, pp. 1278–1287, May 2008.

[2] Z. Zhang, B. Wu, J. Kang, and L. Luo, "A multi-purpose balanced transformer for railway traction applications," *IEEE Trans. Power Del.*, vol. 24, no. 2, pp. 711–718, Apr. 2009.

[3] V. F. Pires, M. Guerreiro, J. F. Martins, and J. F. Silva, "Three-phase multilevel inverter based on LeBlanc transformer," in *Proc. 7th Int. Conf. Workshop Compat. Power Electron.*, 2011, pp. 150–154.

[4] C. Zhao, S. Lewdeni-Schmid, J. Steinke, M. Weiss, and M. Pellerin, "Design implementation and performance of a modular power electronic transformer (PET) for railway application," in *Proc. 14th Eur. Conf. Power Electron. Appl.*, 2011, pp. 1–10.

[5] H. Hu, Z. He, and S. Gao, "Passive filter design for china high-speed railway with considering harmonic resonance and characteristic harmonics," *IEEE Trans. Power Del.*, vol. 30, no. 1, pp. 505–514, Feb. 2015.

[6] G. Celli, F. Pilo, and S. B. Tennakoon, "Voltage regulation on 25 kV ac railway systems by using thyristor switched capacitor," in *Proc. 9th Int. Conf. Harmon. Qual. Power*, 2000, vol. 2, pp. 633–638.

[7] R. Grunbaum, J.-Ph. Hasler, T. Larsson, and M. Meslay, "STATCOM to enhance power quality and security of rail traction supply," in *Proc. 8th Int. Symp. Adv. Electromech. Motion Syst. Electr. Drives Joint Symp.*, 2009, pp. 1–6.

[8] T. Pee-Chin, L. P. Chiang, and D. G. Holmes, "A robust multilevel hybrid compensation system for 25-kV electrified railway applications," *IEEE Trans. Power Electron.*, vol. 19, no. 4, pp. 1043–1052, Jul. 2004.

[9] Y. Mochinaga, Y. Hisamizu, M. Takeda, T. Miyashita, and K. Hasuike, "Static power conditioner using GTO converters for ac electric railway," in *Proc. Conf. Rec. Power Convers. Conf.*, Yokohama, Japan, 1993, pp. 641–646.

[10] Z. Sun, X. Jiang, D. Zhu, and G. Zhang, "A novel active power quality compensator topology for electrified railway," *IEEE Trans. Power Electron.*, vol. 19, no. 4, pp. 1036–1042, Jul. 2004.

[11] Y. Horita, N. Morishima, M. Kai, M. Onishi, T. Masui, and M. Noguchi, "Single-phase STATCOM for feeding system of Tokaido Shinkansen," in *Proc. Int. Power Electron. Conf.*, 2010, pp. 2165–2170.

[12] T. S. Win, B. Yusuke, E. Hiraki, T. Tanaka, and M. Okamoto, "A half-bridge inverter based active power quality compensator using a constant dc capacitor voltage control for electrified railways," in *Proc. 7th Int. Power Electron. Motion Control Conf.*, 2012, vol. 1, pp. 314–320.

[13] Q. Wu, Q. Jiang, and Y. Wei, "Study on railway unified power quality controller based on STATCOM technology," in *Proc. 5th Int. Power Eng. Optim. Conf.*, 2011, pp. 297–300.

[14] B. C. Chen, C. M. Zhang, W. J. Zeng, C. H. Tian, and J. X. Yuan, "An electrical-magnetic hybrid power quality compensation strategy for V/V traction power supply system," in *Proc. IEEE Energy Convers. Congr. Expo.*, 2014, pp. 3774–3779.

[15] A. Luo, C. Wu, J. Shen, Z. Shuai, and F. Ma, "Railway static power conditioners for high-speed train traction power supply systems using three-phase V/V transformers," *IEEE Trans. Power Electron.*, vol. 26, no. 10, pp. 2844–2856, Oct. 2011.

[16] F. Ma *et al.*, "A railway traction power conditioner using modular multilevel converter and its control strategy for high-speed railway system," *IEEE Trans. Transp. Electrif.*, vol. 2, no. 1, pp. 96–109, Mar. 2016.

[17] P. Song *et al.*, "PIR control strategy on compensation of negative sequence and harmonic for railway power supply system using MMC-RPC," *Trans. China Electrotech. Soc.*, vol. 32, no. 12, pp. 108–116, 2017.

[18] Y. Zhao, N. Y. Dai, and B. An, "Application of three-phase modular multilevel converter (MMC) in co-phase traction power supply system," in *Proc. IEEE Conf. Expo Transp. Electrif. Asia-Pac.*, 2014, pp. 1–6.

[19] M. Arabahmadi, M. Banejad, and A. Dastfan, "Hybrid traction power quality compensation system in electrified railway for nominal rating reduction of three-phase converter power switches," in *Proc. 8th Power Electron., Drive Syst. Technol. Conf.*, 2017, pp. 478–483.

[20] L. Luo, Y. Chang, and Y. Li, "A hybrid power conditioner for co-phase power supply system and its capacity analysis," in *Proc. IEEE 3rd Inf. Technol. Mechatron. Eng. Conf.*, 2017, pp. 510–515.

[21] Q. Xu *et al.*, "Analysis and comparison of modular railway power conditioner for high-speed railway traction system," *IEEE Trans. Power Electron.*, vol. 32, no. 8, pp. 6031–6048, Aug. 2017.

[22] Z. Shuai, Y. Hu, Y. Peng, C. Tu, and Z. John Shen, "Dynamic stability analysis of synchronverter-dominated microgrid based on bifurcation theory," *IEEE Trans. Ind. Electron.*, vol. 64, no. 9, pp. 7467–7477, Sep. 2017.

[23] P. C. Tan, P. C. Loh, and D. G. Holmes, "High-performance harmonic extraction algorithm for a 25 kV traction power quality conditioner," *IEEE Proc., Electr. Power Appl.*, vol. 151, no. 5, pp. 505–512, Sep. 2004.

[24] H. J. Kaleybar, M. Fallah, H. M. Kojabadi, S. S. Fazel, and L. Chang, "A new robust dynamic control method for railway power quality compensator," in *Proc. IEEE 8th Int. Power Electron. Motion Control Conf.*, Hefei, China, 2016, pp. 1345–1349.

[25] H. J. Kaleybar and S. Farshad, "A comprehensive control strategy of railway power quality compensator for ac traction power supply systems," *Turk. J. Electr. Eng. Comput. Sci.*, vol. 24, no. 6, pp. 4582–4603, 2016.

[26] F. Ma, Z. He, Q. Xu, A. Luo, L. Zhou, and M. Li, "Multilevel power conditioner and its model predictive control for railway traction system," *IEEE Trans. Ind. Electron.*, vol. 63, no. 11, pp. 7275–7285, Nov. 2016.

[27] J. Min, F. Ma, Q. Xu, Z. He, A. Luo, and A. Spina, "Analysis, design, and implementation of passivity-based control for multilevel railway power conditioner," *IEEE Trans. Ind. Informat.*, vol. 14, no. 2, pp. 415–425, Feb. 2018.

[28] S. V. Emelyanov and V. I. Utkin, "On stability of a class of variable structure systems," *Eng. Cybern.*, no. 2, pp. 115–117, 1964.

[29] V. I. Utkin, "Variable structure systems with sliding modes," *IEEE Trans. Automat. Control*, vol. AC-22, no. 2, pp. 212–222, Apr. 1977.

[30] F. Sebaaly, H. Vahedi, H. Y. Kanaan, N. Moubayed, and K. Al-Haddad, "Sliding mode fixed frequency current controller design for grid-connected NPC inverter," *IEEE J. Emerging Sel. Topics Power Electron.*, vol. 4, no. 4, pp. 1397–1405, Dec. 2016.

[31] J. Ye, P. Malysz, and A. Emadi, "A fixed-switching-frequency integral sliding mode current controller for switched reluctance motor drives," *IEEE J. Emerging Sel. Topics Power Electron.*, vol. 3, no. 2, pp. 381–394, Jun. 2015.

[32] W. Gao and J. C. Hung, "Variable structure control of nonlinear systems: A new approach," *IEEE Trans. Ind. Electron.*, vol. 40, no. 1, pp. 45–55, Feb. 1993.

[33] K. D. Yong, V. I. Utkin, and U. Ozguner, "A control engineer's guide to sliding mode control," *IEEE Trans. Control Syst. Technol.*, vol. 7, no. 3, pp. 328–342, May 1999.

[34] C. Lascu, I. Boldea, and F. Blaabjerg, "Direct torque control of sensorless induction motor drives: A sliding-mode approach," *IEEE Trans. Ind. Appl.*, vol. 40, no. 2, pp. 582–590, Apr. 2004.
[35] B. Beltran, T. Ahmed-Ali, and M. Benbouzid, "High-order sliding-mode control of variable-speed wind turbines," *IEEE Trans. Ind. Electron.*, vol. 56, no. 9, pp. 3314–3321, Sep. 2009.
[36] B. Beltran, T. Ahmed-Ali, and M. E. H. Benbouzid, "Sliding mode power control of variable-speed wind energy conversion systems," *IEEE Trans. Energy Convers.*, vol. 23, no. 2, pp. 551–558, Jun. 2008.
[37] G. Park and Z. Gajic, "A simple sliding mode controller of a fifth-order nonlinear PEM fuel cell model," *IEEE Trans. Energy Convers.*, vol. 29, no. 1, pp. 65–71, Mar. 2014.
[38] A. Luo, F. Ma, C. Wu, S. Q. Ding, Q.-C. Zhong, and Z. K. Shuai, "A dual-loop control strategy of railway static power regulator under V/V electric traction system," *IEEE Trans. Power Electron.*, vol. 26, no. 7, pp. 2079–2091, Jul. 2011.
[39] X. Guo and X. Jia, "Hardware-based cascaded topology and modulation strategy with leakage current reduction for transformerless PV systems," *IEEE Trans. Ind. Electron.*, vol. 62, no. 12, pp. 7823–7832, Dec. 2016.

**Fujun Ma** (M'15) was born in Hunan, China, in 1985. He received the B.S. degree in automation and the Ph.D. degree in electrical engineering from Hunan University, Changsha, China, in 2008 and 2015, respectively.

Since 2016, he has been an Associate Professor with the College of Electrical and Information Engineering, Hunan University. His research interests include power quality managing technique of electrified railway, electric power saving, reactive power compensation, and active power filters.

**Zhen Zhu** was born in Hunan, China, in 1988. He received the B.S. and M.S. degrees in automation from the College of Geophysics and Information Engineering, China University of Petroleum, Beijing, China, in 2013 and 2017, respectively. He has been working toward the Ph.D. degree in electrical engineering at the College of Electrical and Information Engineering, Hunan University, Changsha, China, since 2017.

His research interests include power quality analysis and hybrid compensation control of high-speed railway traction power supply system.

**Jun Min** (S'17) was born in Changsha, China, in 1991. He received the B.S. degree from the College of Information and Electrical Engineering, Hunan Institute of Engineering, Xiangtan, China, in 2014. He is currently working toward the M.S. degree at the College of Electrical and Information Engineering, Hunan University, Changsha, China.

His research interests include power quality management, railway power conditioner, and modular multilevel converter.

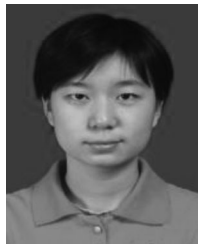

**Yufei Yue** was born in Henan, China, in 1991. She received the B.S. degree in electrical engineering and automation in 2014 from the College of Electrical and Information Engineering, Hunan University, Changsha, China, where she has been working toward the Ph.D. degree in electrical engineering since 2014.

Her research interests include modular multilevel converter and power quality control.

**Xianxian He** was born in Hunan, China, in 1995. She received the B.S. degree from Donghua University, Shanghai, China, in 2016. She is currently working toward the M.S degree at the College of Electrical and Information Engineering, Hunan University, Changsha, China.

Her research interests include modular multilevel converter and power quality management.